JOURNAL OF MATERIALS SCIENCE **34** (1999) 4081–4088

Determination of the fracture mechanical parameters of porous ceramics from microstructure parameters measured by quantitative image analysis

F. VALES*, R. REZAKHANLOU
EDF-DER, Les Renardières, 77250 Moret-sur-Loing, France

C. OLAGNON
INSA-GEMPPM, UMR 5510, 69621 Villeurbanne Cedex
E-mail: christian.olagnon@insa-lyon.fr

The porosity that takes an important part in the failure process of three different ceramic materials (mullite, silicon carbide and silicon nitride) was characterised by means of Quantitative Image Analysis (QIA). Several parameters such as size, shape and orientation of pores have been evaluated. In parallel, the mechanical properties such as fracture toughness and Weibull modulus were directly measured. In order to appreciate the relevance of the use of QIA, the mechanical parameters have also been deduced from the microstructural features, and a comparison between measured and determined values was carried out. The results show a remarkable concordance.

1. Introduction

Since most ceramics do not show plastic deformation at room temperature, they exhibit a brittle behaviour, i.e. the presence of defects governs the mechanical properties. These defects mostly arise from the material processing by powder metallurgy and sintering. Among these different defects, pores of relatively small sizes (usually less than 100 μm) are often the most critical. Therefore the understanding of the ceramic mechanical properties requires the pore distribution characterisation. For this purpose, a possible technique, that has however not been intensively studied in the past, is the Quantitative Image Analysis (QIA). Chermant [1] has applied the QIA to characterise the microstructure of ceramics. The author has presented different types of morphological parameters and has shown how they can be determined by using QIA on sintered materials.

In order to be able to use the information given by a QIA, the relationship between mechanical properties and porosity (or flaws in some cases) distribution must be known. Some models that take into account the reduction of load-bearing area and the stress concentration caused by the pores have been proposed [2] to evaluate the effect of the porosity on strength. The main microstructural parameters were shown to be the volume fraction, the shape and the orientation of the pores.

The aim of the present work is to show that QIA is a relevant technique for microstructural characterisation of some ceramic materials. For this purpose, QIA was first used to determine the porosity content of the material. By applying existing relationships between microstructure and mechanical behaviour, the material mechanical characteristics were further predicted and compared to the same characteristics measured by conventional fracture experiments. The concordance of mechanical parameters values obtained by different mechanical tests and by QIA can validate the use of QIA and the choice of the relationships between microstructure and mechanical parameters. A deterministic approach is also conducted in order to localise before failure, the position of the flaw that will initiate the rupture. A failure criterion is applied to estimate a degree of failure risk.

2. Weibull statistics

2.1. Direct estimation from strength distribution

Since fracture emanates from pre-existing flaws, the strength of ceramic materials generally present a significant scattering. The Weibull statistics is therefore often used to characterise this dispersion. It is generally expressed by the failure probability:

$$F(\sigma) = 1 - \exp\left[-\int\left(\frac{\sigma - \sigma_u}{\sigma_0}\right)^m \mathrm{d}V\right] \qquad (1)$$

* Laboratoire de Mecanique des Solides, UMR7649 Ecole Polytechnique—Route de Saclay—91128 Palaiseau Cedex.

where F is the fracture probability at stress σ, σ_u is the threshold stress, σ_0 is the scale parameter, V the tested volume and m the Weibull modulus. For Brittle materials, σ_u is often equal to zero. The precedent equation can be written as follows:

$$\ln\left(\ln\left(\frac{1}{1-F}\right)\right) = m\ln\sigma - (m\ln\sigma_0 - \ln V) \quad (2)$$

which represents a linear relationship of slope m. A given number, N, of specimens can be tested, for instance in four-point bending. The strengths σ_i are ranked and a probability F_i given by Equation 3, for instance, is attributed:

$$F_i = \frac{i - 0.5}{N} \quad (3)$$

The plot of the curve $\ln(\ln(1/1-F))$ as a function of $\ln(\sigma)$ is fitted to a straight line by linear regression. This can give the different distribution parameters, including the Weibull modulus.

2.2. Estimation by flaw size distribution

Jayatilaka and Tustum [3] have proposed an expression relating the Weibull modulus to the flaw size distribution. It could therefore be directly obtained from the measurement of the flaw size distribution. Image analysis could be a relevant and convenient method to make such a measurement. However, the theory proposed by the authors requires certain condition to be fulfilled:

- an homogeneous flaw distribution,
- the distance between flaws must be large enough to avoid stress interferences,
- the flaw size distribution should be described by a particular law established by Pololniecki and Wilshaw [4]. The probability density of the semi-crack length, $f(a)$ could be fitted with the following expression (see Fig. 1).

$$f(a) = Aa^{-n}\exp\left(\frac{c}{a}\right) \quad (4)$$

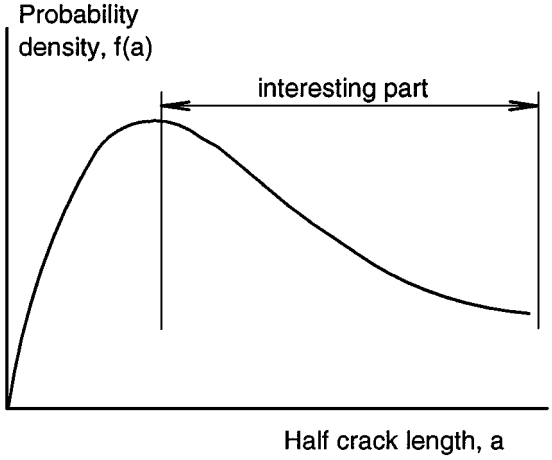

Figure 1 Schematic representation of the half-length defect distribution, $f(a)$.

where A is a geometric constant, c a scaling parameter, a the semi-crack size, n the rate at which the density tends to zero.

It is important to note that the material strength is controlled by the largest flaws i.e. those found in the "tail" of the former curve. Thus, the function describing the crack size distribution for small a, is of no interest for this approach. For a given flaw size distribution (initial conditions and Fig. 1), the theory [3] gives the following relation between the Weibull modulus m and the rate n.

$$m = 2n - 2 \quad (5)$$

On a logarithmic representation and for large sizes, the tail of the distribution becomes linear and n corresponds to the slope. The measurement of n therefore gives directly the Weibull modulus.

3. Quantitative image analysis technique

3.1. Quantitative image analyis parameters

The QIA theory is based on different fields of mathematics such as geometrical probabilities, integral geometry and set transformation [5]. For a given structure, it allows to determine some morphological parameters. In this study, the pores that are considered as fracture initiators are characterised by means of the following morphological parameters:

(i) mean volume fraction of pores,
(ii) size: maximum Feret diameter $2a$ and size distribution (see Fig. 2)
(iii) shape: (see Fig. 2)

- *total surface*, S,
- *circularity factor*, C, defined as the ratio of the total surface to the square perimeter P as follows:

$$C = \frac{4\pi S}{P^2} \quad (6)$$

For a circle, $C = 1$.

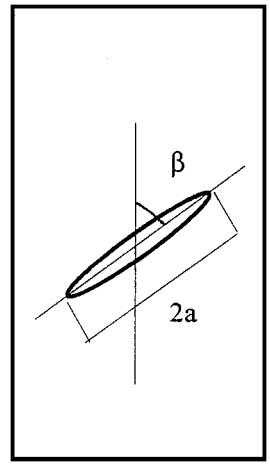

Figure 2 Description of the flaw parameters recorded by image analysis.

- *inclination angle* between the maximum Feret diameter and a reference direction chosen as the longest beam length.

3.2. QIA procedure

The primary image (either from optical or scanning electron microscope) must be treated to reduce the quantity of information. For this purpose, it is digitised and in some cases improved using a grey tone treatment. It is further thresholded to obtain a binary image in order to separate what corresponds to the phase to be measured (here the pores) from the rest of the image (dense material). The major difficulty at that step is to eliminate excessive noise or large zones of excessive brightness. This can be done by means of filters, allowing feature smoothing and small size particle elimination.

For a given structure, some parameters conditions are perquisite. The measurement parameters must be independent of the measurement scale. The investigation field must be of a significant size compared to the whole structure in order to obtain relevant data. An additional problem is the extrapolation of the bidimensional space measurement to three dimension structure. This can be done by means of stereology approach that allows to establish relationships between both spaces. Finally for any image analysis method, it should be controlled that the investigated surfaces are representative of the material bulk.

3.3. Relationship between mechanics and QIA parameters

According to the brittle fracture approach, the critical flaw initiating the rupture is generally that submitted to a tensile stress field that owing to a specific arrangement between the size and the orientation (Fig. 2) exhibits the highest stress intensity factor. The most critical size is the largest one, and the most critical orientation is when the applied direction and the flaw direction (direction of the maximum Feret diameter) nearly define a right angle. Jayatilaka and Trustum [3] give a relation between the flaw parameters and the material property:

$$K_{IC}^2 = 2\sigma^2 a\beta \tag{7}$$

where K_{IC} is the critical stress intensity factor, σ is the fracture strength, a is the semi-crack length and β is the angle between the applied load direction and the flaw direction. In order to separate material and flaw parameters, Equation 7 can be written:

$$\frac{K_{IC}}{\sigma} = \sqrt{2a\beta} \tag{8}$$

The factor $\sqrt{2a\beta}$ is available by image analysis during the morphological characterisation (see Section 3.1). Fracture toughness is a material constant (determined in Section 4.3), so the fracture strength can be estimated. The critical zone exhibits the lowest fracture strength i.e. the largest factor $\sqrt{2a\beta}$. The values of this factor therefore gives a criterion to localise the most critical flaw before fracture.

4. Experimental

4.1. Materials

Three ceramic materials of different characteristics have been used for this investigation. Two technical ceramics: a mullite and a silicon nitride, and a coarse microstructure silicon carbide. The mullite (Céramique et Composites, Bazet, France) processed by pressing shows a relatively small grain size of 5 μm. Pores of maximum size equal to about 50 μm (see Fig. 3) have also been observed. The silicon nitride was a

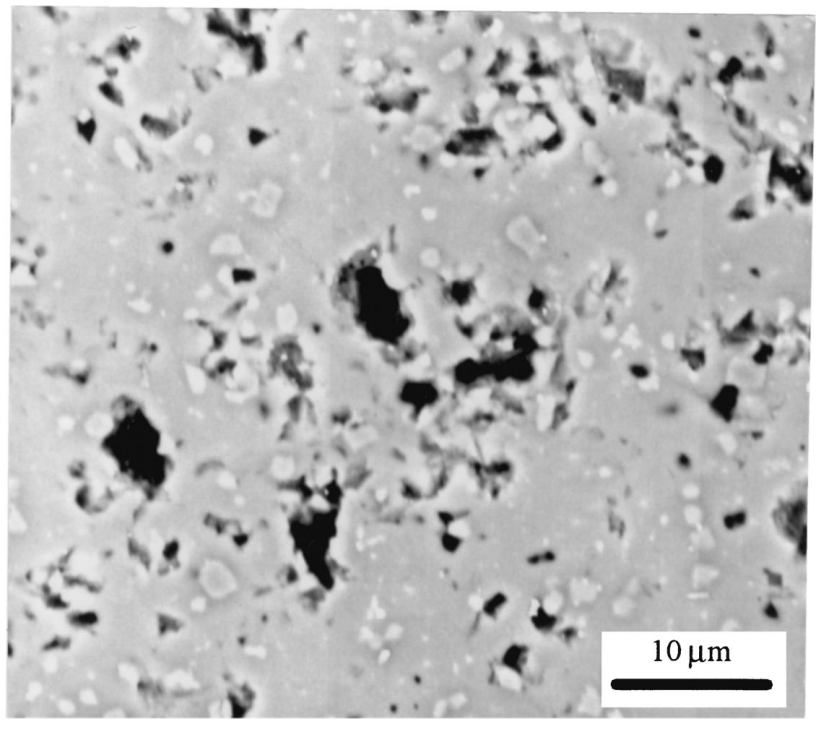

Figure 3 Back scattered SEM micrograph of the mullite microstructure used for image analysis.

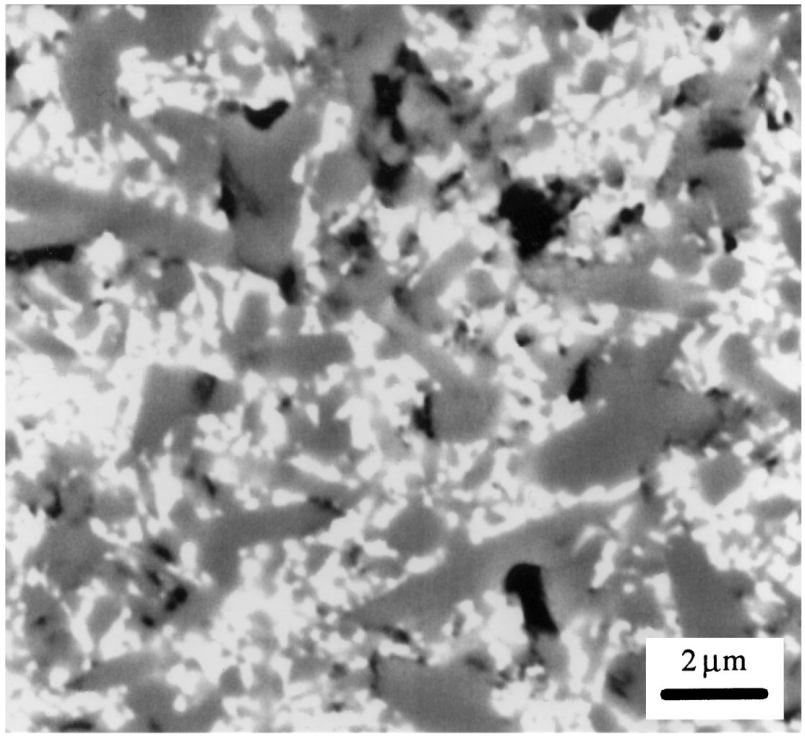

Figure 4 Back scattered SEM micrograph of the silicon nitride microstructure used for image analysis.

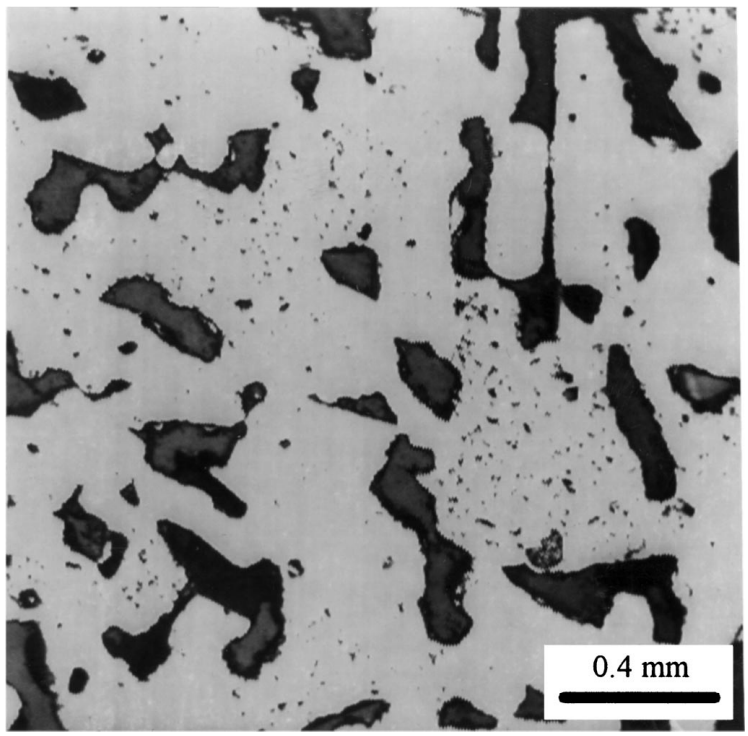

Figure 5 Optical micrograph graded in grey levels of the silicon carbide microstructure.

nearly dense Sintered Reaction Bonded Silicon Nitride (SRBSN, ESK, Germany). The microstructure is also relatively fine-grained with small pores, evenly distributed. Some residual silicon is present (about 4%). The β-Si_3N_4 grains present an acicular shape with a diameter between 1 to 5 μm (Fig. 4).

The silicon carbide (Crystar CS501, Norton, England) was obtained by direct sintering from the initial powder. The coarse microstructure with large pores and grain sizes (up to 500 μm) can be analysed by optical microscopy (Fig. 5).

4.2. Image analysis procedure

An image treatment is only relevant for one type of image (similar level of brightness, contrast and noise). Thus, a particular analysis procedure must be developed for each material and for a given magnification.

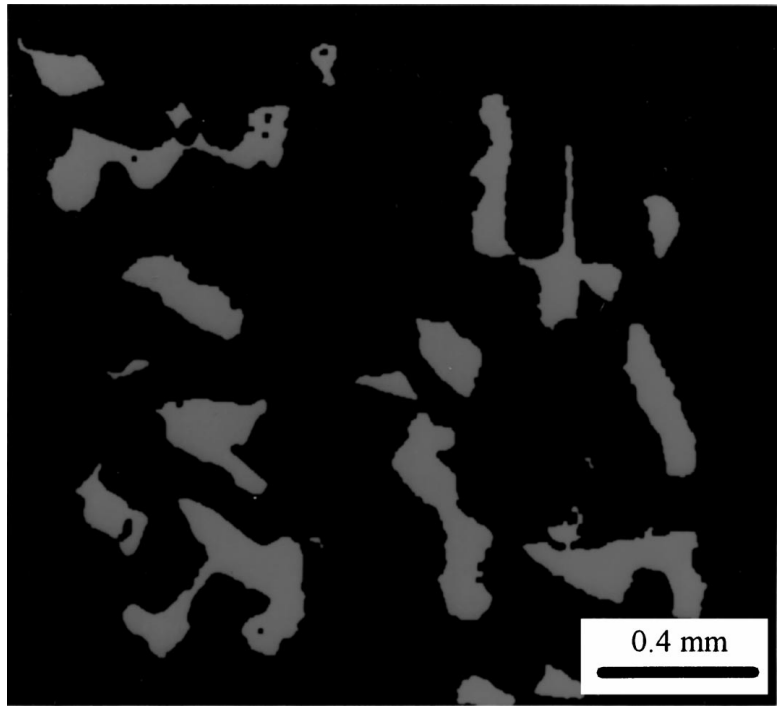

Figure 6 Silicon carbide pores selected from Fig. 5 after the image treatment.

In addition, the image treatment to be conducted will strongly depend on the type of information needed to be recorded.

The image analysis equipment includes a microscope (optical or scanning electron) fitted out with a camera and an automatic image analyser produced by Matra (MSII Pericolor 2001). This includes a threshold, a logic and a measurement unit.

The different analysis steps can be summarised as:

(i) Image acquisition from the microscope. The image is composed of 256 grey levels (Fig. 4).

(ii) Digitalisation: the initial image is digitised and thresholded to obtain a binary image.

(iii) Image treatment: opening and closing series are used in order to "clean" the image and to keep the only necessary information.

(iv) Porosity volume fraction is evaluated by specific surface area measurement.

(v) Edge effects: along the edges of the observation field, some pores are partially hidden (Fig. 6). They should be eliminated since the exact size can not be obtained. The choice of magnification is therefore important because in a given field, pores should be large enough to be characterised but small enough to reduce this edge effect.

(vi) Morphological parameter measurements.

The analyses were conducted on four point bending samples (see Section 4.3). For a given material, the specimens were split into two different batches. The first group of specimens was previously fractured in bending. In such a case, the cross-section of the bars were analysed. The tensile faces of the SiC materials were also investigated. The second group of specimens was first image analysed and subsequently tested in bending. In this case, only the tensile face was explored.

The main error arising in the image analysis concerns the image acquisition and the brightness adjustment of the microscope and the camera. For an optical microscope, the porosity volume fraction can be measured with an accuracy of about 1.5%. When using the SEM, the error was even smaller and considered as insignificant.

4.3. Mechanical parameter estimation procedure

Several methods can be used to measure the fracture toughness. The first solution consists in introducing an artificial surface flaw on the tensile side, such as a notch or an indentation crack, and in fracturing the notched beam. The fracture initiates from this flaw because it is the most critical in the specimen. One of the advantages is that artificial flaw size can be easily measured. A direct measurement method can also be possible by measuring the crack length resulting from indentation of a specimen under a given load.

An alternative technique consists in measuring the sizes of natural flaws on the tensile sides of the beams. The technique of image analysis is in this case particularly suited. In order to show the validity of the QIA techniques different toughness measurements have been conducted, as detailed below:

(i) Fracture of notched bending specimens has been applied with two different starting flaws. On one hand, single edge notch (SENB) was made on the tensile face with a diamond saw (0.3 mm width). The notch was nearly 40 percent of the beam depth. The toughness was calculated from the critical value of the stress intensity factor at rupture using the expression given by Tada [6] for pure bending.

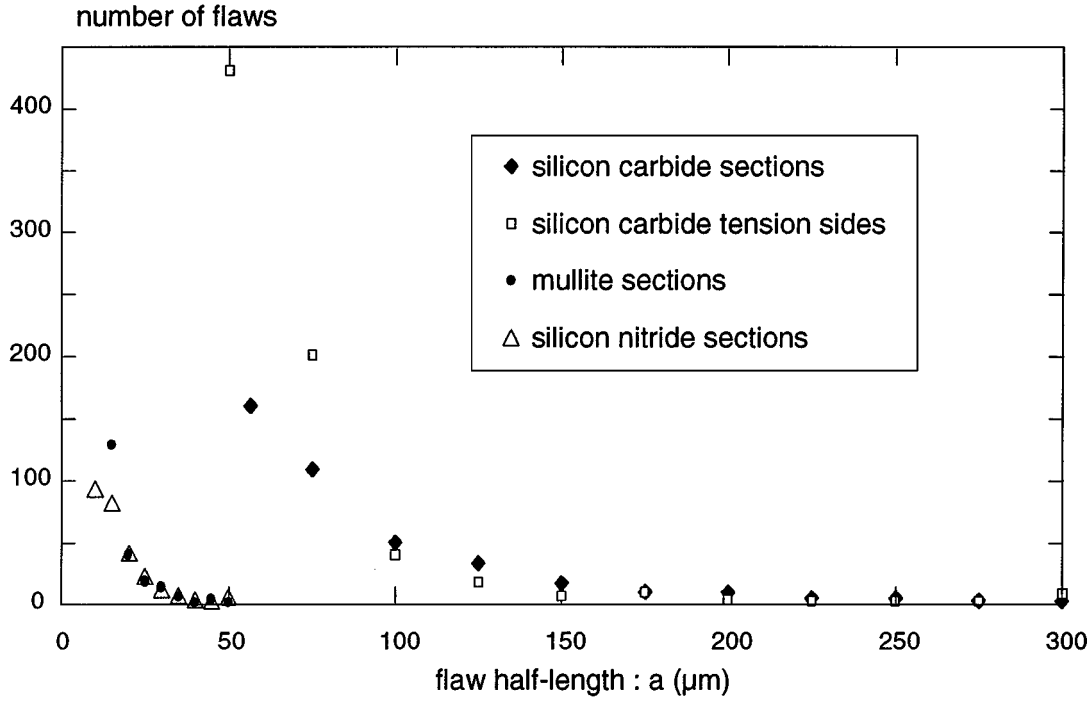

Figure 7 Experimental distribution of the half-length size of pores a for the three materials, as measured by image analysis.

On the second hand, artificial flaws were made by Vickers indentation [7]. An annealing treatment was made to eliminate the residual stress introduced by indentation. Since the indentation flaws are semi-elliptical, the critical stress intensity factor K_{IC} has been calculated by using Murakami expression [8].

(ii) The fracture toughness has also been measured by the direct measurement method [9]. The polished surface of the specimens were indented by means of a Vickers hardness diamond. From the applied load, P the Young modulus E and the half-crack length a, the fracture toughness can be estimated. Fracture toughness values are calculated using Shetty [10] formula:

$$K_{IC} = 0.0889\left(\frac{HP}{4l}\right)^{1/2} \tag{9}$$

where l is the difference between the semi-sharp crack length and the half diagonal length of the print, and H the hardness.

For the mullite ceramic, the applied load was 40 N and the Young modulus in bending was measured as 180 GPa. For the silicon nitride material, the values were respectively $P = 200$ N and $E = 280$ GPa. This direct technique could not be conducted on the SiC material owing to its coarse microstructure.

(iii) Fracture toughness estimation by QIA. The beams were tested in four point bending and the tensile sides were subsequently analysed. Natural flaws (pores) were characterised by their size. Note that the flaw that initiated the fracture, is not accessible because it is located in the fracture surface plane. But the "second most critical flaw" can be detected.

The Weibull modulus was measured by the two methods presented in Section 2, i.e. from the porosity size distribution measured by QIA and from mechanical tests. In the last case 20 specimens were tested in order to obtain a relevant Weibull modulus value.

The mechanical tests (for Weibull and toughness measurements) were conducted in four point bending at room temperature. The specimens were of parallelepiped shape with dimensions $45 \times 4 \times 3$ mm^3. The tensile surface of the bars was polished in order to eliminate surface flaws resulting from machining. The edges of the polished sides were bevelled. The tests were conducted on a tensile machine at an imposed cross-head speed of 0.5 mm/min.

4.4. Deterministic approach

A tentative of failure location prediction from the systematic analysis of some specimens by QIA has also been conducted. This has only been conducted on 5 samples of the silicon carbide. The coarse microstructure of this material allowed an easier and faster analysis than the two other one. The tensile side of the bending bars were analysed before fracture. For each bar, 22 fields have been explored as shown in Fig. 8 and the

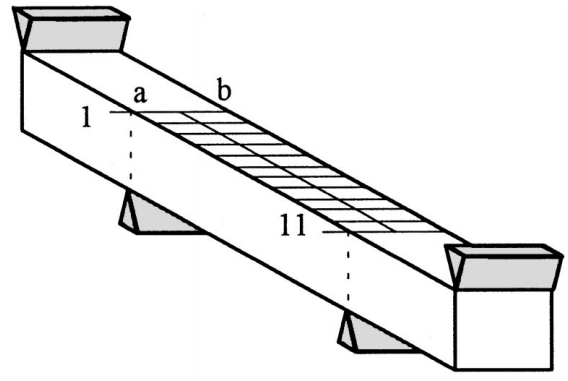

Figure 8 Schematic drawing of the QIA procedure for the deterministic approach.

factor $\sqrt{2a\beta}$ was calculated. For each specimen, the zone containing the highest value, i.e. the most critical defect, was localised. The specimens were further tested in four-point bending and the fracture zone localisation were compared to the predictions.

5. Results and discussion

5.1. Porosity characterisation

5.1.1. Volume fraction

Two methods were used to measure the porosity volume fraction. The first technique is the image analysis on polished surface. The second consisted of measuring the bulk density. For this purpose, the weight of the samples was determined and the total volume was calculated from the dimensions. The theoretical density was estimated using the weight fraction and the density of each phase present in the material. The porosity volume fraction was evaluated as the difference between the measured bulk density and the theoretical density rationalised by the theoretical density. The results are given in Table I. Both methods showed a remarkable agreement. This validated the image analysis procedure and the accessibility of a volume parameter estimation from a surface measurement.

5.1.2. Morphological parameters

One of the most important advantage of QIA is to allow a defect size measurement statistical approach. Since large size pores take part in fracture mechanisms, only these flaws were studied. The tail of the porosity size distribution measured by QIA is reported in Fig. 7. For the different tested materials, the shape of the curve is the same with pore sizes different for each material. The maximum values of the half length of the pores are given in Table II.

5.2. Toughness and fraction location

The different measured fracture toughness values are reported in Table III. The several classical measurement methods give similar results except for the indentation

TABLE I Porosity volume fraction estimations

Materials	Theoretical density ($g \cdot cm^{-3}$)	Porosity determined by weight method (%)	Porosity determined by image analysis (%)
Silicon carbide	3.3	22 ± 0.8	21 ± 3
Mullite	3.2	7.5 ± 1.8	5.2 ± 1.5
Silicon nitride	3.4	3.7 ± 1	4 ± 1.3

TABLE II Maximum half-length of pores, a

Materials	Microscope type	Magnification	Max. half-length (a in μm)
Silicon carbide	Optical	100	500
Mullite	SEM	2000	77
Silicon nitride	SEM	7000	53

TABLE III Fracture toughness measurements

Materials	Image analysis MPa $m^{1/2}$	SENB MPa $m^{1/2}$	Vickers indentation MPa $m^{1/2}$	Direct measurement MPa $m^{1/2}$
Silicon carbide	3.3 ± 0.5	2.6 ± 0.2	—	—
Mullite	2.5 ± 0.5	2.6 ± 0.2	1.6 ± 0.2	2.6 ± 0.1
Silicon nitride	7 ± 1	7.7 ± 0.3	6.6 ± 0.3	6.9 ± 0.3

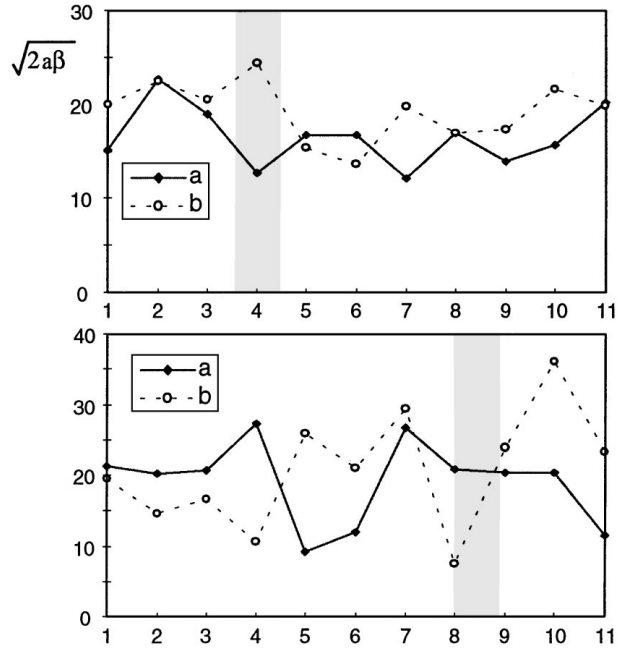

Figure 9 Two examples of $\sqrt{2a\beta}$ factor estimation on tensile side of a bending bar. The shaded area indicates the observed fracture location.

mullite beams where K_{IC} is underestimated, suggesting that the residual stresses have not been fully annealed. The agreement with the values obtained by image analysis is very fair, suggesting that it might be a reliable technique.

The analysis of the so-called deterministic approach was less successful. The comparison of the failure location to the failure prediction showed that only about 40% of the specimens could be predicted. Two examples are given in the Fig. 9. This shows that the selected criterion is not fully relevant. Other factors such as the depth or the shape in the fracture plane play a role on the failure stress. A definite deterministic approach for such a case is not possible. However, the image analysis investigation conducted in this example could be used in terms of failure probability.

5.3. Weibull modulus

The Weibull modulus estimated by both methods are reported in Table IV. Modulus determinations from surface analysis and from mechanical tests, provide the same results except for the measurements made on silicon carbide sections. However, in this last case, the analysis of the tensile sides leads to correct Weibull modulus values. This suggests that the flaw distribution is not homogeneous in the silicon carbide. The most critical flaws appeared as located on the tensile

TABLE IV Weibull modulus values determined by different methods

Materials	Analysed surfaces	Weibull modulus (image analysis)	Weibull modulus (mechanical tests)
Silicon carbide	Beam sections	5 ± 1	10 ± 2.2
	Tensile sides	11 ± 1	
Mullite	Beam sections	12 ± 1.5	13 ± 1.6
Silicon nitride	Beam sections	5.5 ± 1	7 ± 1.6

face, i.e. on the surface. The reason in not clear, but it might be due to machining that could have modified the flaw distribution.

6. Conclusion

The QIA allows to characterise the porosity that represents the critical flaws in many ceramics. In the different materials investigated here, it has been possible to obtain relevant values of the density, the fracture toughness and of the Weibull modulus from the analysis of the porosity on the surfaces. These results showed a good agreement with values measured by standard mechanical tests. The possibility to obtain the Weibull modulus from the geometrical parameters of the flaws, confirms the theory of Jayatilaka and Trustum [3]. The QIA can therefore be an interesting technique to characterise the flaws (volume fraction, size distribution, shape parameters) and presents the advantage to be a non destructive method. However, an extensive industrial application of the technique still appears as difficult. The main disadvantages of QIA are the need of a specific image treatment for each material and each magnification and the difficulty to estimate the measurement error.

References

1. J. L. CHERMANT, *Ceramics International* **12** (1986) 67–80.
2. A. R. BOCCACCINI and G. ONDRACECK, Third Euro-Ceramics, edited by P. Duran and J. F. Fernandez (Faenza, Spain, 1993) vol. 3, pp. 895–900.
3. A. DE S. JAYATILAKA and K. TRUSTUM, *J. Mater. Sci.* **12** (1977) 1426–1430.
4. J. D. POLONIECKI and T. R. WILSHAW, *Nature Physical Science* **229** (1971) 226–227.
5. M. COSTER and J. L. CHERMANT, Précis d'analyse d'images, Presses du CNRS, France, 1989, pp. 1–12, 364–368.
6. H. TADA, The Stress Analysis Handbook, Paris production Incorporated, 1985.
7. J. J. PETROVIC and M. G. MENDIRATTA, Fracture from controlled surface flaws, fracture mechanics applied to brittle materials, Freiman editor, ASTM STP678, 1979, pp. 83–102.
8. Y. MURAKAMI, "Stress Intensity Factor Handbook," Vol. (Pergamon Press, 1987), pp. 723–724.
9. D. B. MARSHALL and B. R. LAWN, "Indentation of brittle materials, microindentation techniques in Material Science and Engineering," ASTM STP 889, edited by P. J. Blau and B. R. Lawn (American Ceramic Society for testing an materials, Philadelphia, 1986) pp. 26–46.
10. D. K. SHETTY, I. G. WRIGHT, P. N. MINCER and A. H. CLAUER, *J. Mater. Sci.* **20** (1985) 1873–1882.

Received 2 January 1997
and accepted 14 January 1999